Right-handed weak currents in neutrinoless $\beta\beta$ decays and ton-scale $\beta\beta$ detectors

Hiroyasu Ejiri,* Takeshi Fukuyama,† and Toru Sato‡
Research Center for Nuclear Physics, Osaka University, Osaka 567-0047, Japan

(Received 13 January 2025; revised 13 April 2025; accepted 20 May 2025; published 13 June 2025)

Right-handed weak currents (RHCs) in the left-right symmetric model for neutrinoless double beta decays (DBDs) of both the $0^+ \rightarrow 0^+$ and $0^+ \rightarrow 2^+$ transitions are discussed from both theoretical and experimental viewpoints. $\langle\lambda\rangle$ and $\langle\eta\rangle$ terms are related by $\langle\lambda\rangle/\langle\eta\rangle \approx \tan\beta$, which is constrained in the regions of 1–60 for SUSY grand unified theories (GUTs) and of 1–165 for non-SUSY GUTs. The enhancement mechanisms of the $\langle\eta\rangle$ term over the $\langle\lambda\rangle$ term in the 0^+ transition is shown, and the Δ isobar contribution to the nuclear matrix element (NME) for the transition to the 2^+ state is found to be of the order of 20% of the NME with the quenched weak coupling. The new and interesting RHC regions of $\langle\lambda\rangle \approx 5 \times 10^{-8}$ and $\langle\eta\rangle \approx 1.5 \times 10^{-10}$ are shown to be exclusively explored by measuring both the $\beta\beta$ and γ rays associated with the ground and excited DBDs by means of the ton-scale DBD detectors for the inverted hierarchy ν masses. The actual RHCs to be studied depend on the RHC NMEs.

DOI: 10.1103/f4cf-vnr9

I. INTRODUCTION

Neutrinoless double beta decay (DBD) is a realistic probe for studying the neutrino (ν) nature (Majorana or Dirac), the absolute ν mass scale, the right-handed weak current (RHC), and others, which are beyond the standard model (BSM), as discussed in reviews [1–5] and references therein.

In the present work we study the effects of the RHC in the 0ν DBDs to the ground and excited states, where $\langle\lambda\rangle$ and $\langle\eta\rangle$ terms in addition to $\langle m\rangle$ terms appear [Eq. (12)]. Based on the neutrino oscillation experiments, the effective Majorana neutrino-mass $\langle m\rangle$ is around 15–45 meV and 2–5 meV for the inverted mass hierarchy (IH) and the normal mass hierarchy (NH) cases, respectively. The recent experimental works are concentrated mostly on the light-mass mechanism by measuring the ground-state $0^+ \rightarrow 0^+$DBDs [6,7].

The DBD transition rate depends on the nuclear matrix element (NME). The NME, which reflects the complex nuclear correlations in the DBD nucleus, is crucial to extract the ν mass and the contributions of RHCs. The NME, however, depends on the models and the nuclear parameters used there [8–12]. One critical parameter is the effective axial-vector weak coupling $g_A^{\rm eff}$, which is much quenched in a nucleus due to the various kinds of nucleonic and non-nucleonic correlations [13–16].

Recent high-sensitivity experiments have excluded the larger ν mass region of $\langle m\rangle \geqslant$ 100–200 meV, depending on the NME. Then they are going to build higher-sensitivity and larger-scale DBD detectors to search for the neutrino mass in the IH neutrino-mass region around $\langle m\rangle \approx 30$ meV. Since the minimum neutrino mass to be measured is proportional to $(B/N)^{1/4}$ with N being the total amounts of the DBD isotopes used in the detector and B being the backgrounds, one needs ton-scale ($N \approx$ tons) detectors to measure the IH neutrino mass and even multi-10 ton scale DBD detectors for the NH neutrino mass. Accordingly, one might anticipate that the ton-scale DBD detectors under construction may not be quite effective if the neutrino mass spectrum is of NH without RHC.

From the theoretical view point of grand unified theories (GUTs), our results prefer the NH to the IH: that is, inputting the observed lepton masses and the Pontecorvo–Maki–Nakagawa–Sakata (PMNS) angles into the model, we compare the outputs of quark masses and CKM matrices in the model with the observed data, and obtained $\chi^2 \leqslant 1$ for the NH case and $\chi^2 > 200$ for the IH case [17]. On the other hand, recent measurements of baryonic acoustic oscillations of cosmic microwave background constrain [18–20] $\sum_i m_{\nu i} < 0.072$ eV at 95% C.L. This bound disfavors IH at 3σ [21]. If this is the case, the future ton-scale DBD detectors may find no ν mass signals but the RHC ones [22].

DBD experiments, so far, have been made mostly for the ground 0^+ state with the large phase space factors. In fact, the DBD phase space and thus the DBD rate for the excited 2^+ state are much smaller than those for the ground state, and in any way the ν mass term does not contribute to the excited-state transition as discussed later. Here we note that the excited-state DBD is characterized by the γ ray from the excited state.

The present paper aims to report the theoretical aspects of the RHCs and the RHC regions to be studied by measuring

*Contact author: ejiri@rcnp.osaka-u.ac.jp
†Contact author: fukuyama@rcnp.osaka-u.ac.jp
‡Contact author: tsato@rcnp.osaka-u.ac.jp

Published by the American Physical Society under the terms of the Creative Commons Attribution 4.0 International license. Further distribution of this work must maintain attribution to the author(s) and the published article's title, journal citation, and DOI. Funded by SCOAP³.

both DBDs to the ground and excited states with the ton-scale DBD detectors for both the $\beta\beta$ and γ rays. The RHCs to be studied are $\langle\lambda\rangle$ and $\langle\eta\rangle$ in the regions of the orders of 10^{-8} and 10^{-10}, respectively. Then the DBD signal in the 0^+ ground state is due to either $\langle\lambda\rangle$ or $\langle\eta\rangle$, or both of them, while that in the 2^+ one is exclusively due to $\langle\lambda\rangle$, as will be discussed in Secs. III and IV. From these experiments, one obtains the values for the ratio $\langle\lambda\rangle/\langle\eta\rangle$, which is related to $\tan\beta$, and the parameters included in the RHC mechanisms in BSM physics.

DBD detectors to be discussed in the present work are $\beta\beta$-γ detectors to make it possible to separate the excited-state decay from the ground-state decay and to reduce considerably background contributions to both the ground- and excited-state DBD studies, as shown in early works with ELEGANT experiments [23,24]. Actually, DBD detectors used so far for high-sensitivity DBD experiments are mostly calorimetric detectors to measure the total DBD energy, but do not measure individual 2β-ray tracks to identify the DBD processes, the mass, λ, and η ones.

This paper is organized as follows: The theoretical aspects of the RHC DBD are discussed briefly in Sec. II. The RHC NMEs for the 0^+ ground- and 2^+ excited-state transitions are discussed in Sec. III. Here we include brief discussions on the possible contribution of the Δ isobar to the RHC NMEs to the 2^+ excited state. Experimental sensitivities for measuring the λ and η RHCs and experimental merits of measuring both $\beta\beta$ and γ rays are explained in Sec. IV. Finally, concluding remarks on the future RCH DBD works are given in Sec. V.

II. THEORETICAL ASPECTS OF RIGHT-HANDED WEAK CURRENT DOUBLE BETA DECAYS

In discussing the theoretical models for 0ν DBD, the most important thing is how to make a neutrino mass. There are two approaches: The first is the introduction of right-handed current, and the second is the radiative generation of neutrino mass, both of which explain why neutrino mass is much lighter than the other charged leptons and quarks. That is, the former is due to the seesaw mechanism and the latter to the loop factor $(16\pi^2)^{-n}$ for n loops [25]. Unfortunately, there are too many varieties of model options for the latter case. On the other hand, in the former case, RHC, has the firm root in GUT [26] and is able to get the restrictions and correlations in BSM physics like lepton number, flavor violations, etc. Therefore, in this paper, we stand on the RHC scenario. We use the notations of Ref. [27] for the detailed applications of the left-right (L-R) symmetric model. The weak Hamiltonian is given by

$$H_W = \frac{G_F\cos\theta_c}{\sqrt{2}}\left[j_{\rm L}^{\mu}\tilde{J}_{{\rm L}\mu}^{\dagger} + j_{\rm R}^{\mu}\tilde{J}_{{\rm R}\mu}^{\dagger}\right] + {\rm H.c.} \tag{1}$$

Here j_μ (J_μ) indicates the leptonic (hadronic) current, and the L- and R-handed leptonic currents $j_{{\rm L}\mu}$ and $j_{{\rm R}\mu}$ are given by

$$\begin{aligned} j_{{\rm L}\alpha} &= \sum_{l=e,\mu,\tau}\overline{l(x)}\gamma_\alpha(1-\gamma_5)\nu_{lL}(x) \\ &\equiv \sum\overline{l(x)}\gamma_\alpha 2P_L\nu_{lL}(x), \end{aligned} \tag{2}$$

$$\begin{aligned} j_{{\rm R}\alpha} &= \sum_{l=e,\mu,\tau}\overline{l(x)}\gamma_\alpha(1+\gamma_5)N_{lR}(x) \\ &\equiv \sum\overline{l(x)}\gamma_\alpha 2P_R N_{lR}(x), \end{aligned} \tag{3}$$

where $\nu_{lL}(N_{lR})$ are L-handed (R-handed) weak eigenstates of the neutrinos, and

$$\tilde{J}_{\rm L}^{\mu}(\boldsymbol{x}) = J_{\rm L}^{\mu}(\boldsymbol{x}) + \kappa J_{\rm R}^{\mu}(\boldsymbol{x}), \tag{4}$$

$$\tilde{J}_{\rm R}^{\mu}(\boldsymbol{x}) = \eta J_{\rm L}^{\mu}(\boldsymbol{x}) + \lambda J_{\rm R}^{\mu}(\boldsymbol{x}). \tag{5}$$

The neutrino mass matrix is [28–31]

$$M_\nu = \begin{pmatrix} M_L & M_D^T \\ M_D & M_R \end{pmatrix} \approx \begin{pmatrix} 0 & M_D^T \\ M_D & M_R \end{pmatrix}. \tag{6}$$

Thus, we have the extended Fermi couplings (1). In (2) and (3), $\nu_{lL}(N_{lR})$ are L-handed (R-handed) weak eigenstates of the neutrinos. Using 3×3 blocks U, V, X, Y, the mass eigenstates ν', N' are given as

$$\begin{pmatrix} \nu \\ (N_R)^c \end{pmatrix}_L = \begin{pmatrix} U & X \\ V^* & Y \end{pmatrix}\begin{pmatrix} \nu' \\ N' \end{pmatrix}_L \equiv \mathcal{U}\begin{pmatrix} \nu' \\ N' \end{pmatrix}_L. \tag{7}$$

That is,

$$(\nu_L)_\alpha = U_{\alpha i}\nu_i' + X_{\alpha I}N_I', \qquad (N_R)_\alpha^c = V_{\alpha i}^*\nu_i' + Y_{\alpha I}N_I', \tag{8}$$

where α (i) are the flavor (mass) eigenstates:

$$\mathcal{U}^T M_\nu \mathcal{U} = \begin{pmatrix} m_{\rm light} & 0_{3\times 3} \\ 0_{3\times 3} & M_{\rm heavy} \end{pmatrix}, \tag{9}$$

$$m_{\rm light} = -M_D^T M_R^{-1} M_D. \tag{10}$$

From GUT, if we adopted a very naive order estimation neglecting flavor indices, M_D is of the order of the top quark mass, M_R is of the order of 10^{14} GeV, and the effect of RHC is not observable. However, we can realize the TeV-scale seesaw [32] in the $\mathrm{SU}(2)_L\times\mathrm{SU}(2)_R\times\mathrm{U}(1)_{B-L}$ model [33]. The transition rate (inverse of the half-life $T_{1/2}^J$) for $0^+\to J^+$ ($J=0,2$) is given as [1,8,11,34–36]

$$\begin{aligned} \Gamma^{(J)} \equiv \frac{1}{T_{1/2}^J} &= C_{mm}^{(J)}\left(\frac{\langle m\rangle}{m_e}\right)^2 + C_{m\lambda}^{(J)}\frac{\langle m\rangle}{m_e}\langle\lambda\rangle \\ &+ C_{m\eta}^{(J)}\frac{\langle m\rangle}{m_e}\langle\eta\rangle + C_{\lambda\lambda}^{(J)}\langle\lambda\rangle^2 \\ &+ C_{\eta\eta}^{(J)}\langle\eta\rangle^2 + C_{\lambda\eta}^{(J)}\langle\lambda\rangle\langle\eta\rangle. \end{aligned} \tag{11}$$

Here $C_{ab}^{(0)}$ includes the NME and the phase-space integral. The other parts include the ν mass and the BSM physics. The effective couplings $\langle\eta\rangle$ and $\langle\lambda\rangle$ are given as

$$\begin{aligned} \langle m\rangle &= \left|\sum_i U_{ei}^2 m_i\right|, \quad \langle\lambda\rangle = \lambda\left|\sum_j U_{ej}V_{ej}\right|, \\ \langle\eta\rangle &= \eta\left|\sum_j U_{ej}V_{ej}\right|. \end{aligned} \tag{12}$$

The constants λ and η in (1) are related to the mass eigenvalues of the weak bosons in the L- and R-handed gauge

sectors (W_L, W_R) as follows [37]:

$$W_L^+ = W_1^+ \cos\zeta - W_2 \sin\zeta e^{-i\alpha}, \tag{13}$$

$$W_R = W_1^+ \sin\zeta e^{i\alpha} + W_2^+ \cos\zeta, \tag{14}$$

$$\frac{G_F}{\sqrt{2}} = \frac{g^2}{8}\cos^2\zeta \frac{M_{W1}^2 \tan^2\zeta + M_{W2}^2}{M_{W1}^2 M_{W2}^2}, \tag{15}$$

$$\lambda = \frac{M_{W1}^2 + M_{W2}^2 \tan^2\zeta}{M_{W1}^2 \tan^2\zeta + M_{W2}^2}, \tag{16}$$

$$\eta = -\frac{\left(M_{W2}^2 - M_{W1}^2\right)\tan\zeta}{M_{W1}^2 \tan^2\zeta + M_{W2}^2}. \tag{17}$$

Here M_{W1} and M_{W2} are the masses of the mass eigenstates W_1 and W_2, respectively, and ζ is the mixing angle which relates the mass eigenstates and the gauge eigenstates. We are considering the L-R symmetric model. The gauge boson masses are [37]

$$M_W^2 = \begin{pmatrix} \frac{1}{2}g^2\left(\kappa^2 + \kappa'^2 + 2v_L^2\right) & -g^2\kappa\kappa' e^{-i\alpha} \\ -g^2\kappa\kappa' e^{i\alpha} & g^2 v_R^2 \end{pmatrix}. \tag{18}$$

Here the Yukawa coupling between quark doublets (and lepton doublets) and bi-doublet Higgs is given by

$$\mathcal{L}_Y = \overline{Q}_{Li}(Y_{ij}\Phi + Y'_{ij}\tilde{\Phi})Q_{Rj} + \text{H.c.}, \tag{19}$$

with

$$\langle\Phi\rangle = \begin{pmatrix} \kappa & 0 \\ 0 & \kappa' e^{i\alpha} \end{pmatrix}, \quad \text{and} \quad \tilde{\Phi} = \tau_2\Phi^*\tau_2. \tag{20}$$

Thus, this model is the "minimal" L-R symmetric model. In this mode, there are loop diagrams to generate 0ν DBD other than the three tree diagrams [25,27]. However, it is subdominant compared with the above three tree diagrams. We consider this model to clarify the essence of L-R symmetric model in DBD. However, the quark mixing angle is almost diagonal, and if we assume

$$\kappa \gg \kappa', \quad \text{and} \quad Y_{ij} \gg Y'_{ij}, \tag{21}$$

then they are related to more familiar quantities,

$$\kappa \approx v_u, \quad \kappa' \approx v_d, \quad \frac{1}{\sqrt{2}}(\kappa^2 + \kappa'^2) = v_{ew}^2. \tag{22}$$

Then the L-R weak boson mixing angle becomes

$$\tan 2\zeta = -\frac{2\kappa\kappa'}{v_R^2} \approx \frac{2v_u v_d}{v_R^2} = -4\xi\left(\frac{M_{WL}}{M_{WR}}\right)^2, \tag{23}$$

with [38]

$$\xi \equiv \kappa'/\kappa \approx v_d/v_u \equiv 1/\tan\beta, \tag{24}$$

and [39]

$$M_{W2} = g_R v_R \geqslant 3.7 \text{ TeV}, \tag{25}$$

where the symbol $\approx$ implies adopting the assumption of (21). In the L-R symmetric model, we set $g_L = g_R$, which indicates further unification of at least rank five GUT, including SU(3) color. The function $\tan\beta$ is constrained by the fact that the Yukawa coupling is renormalizable up to the GUT scale,

$$1 \leqslant \tan\beta \leqslant \begin{cases} 60 & \text{SUSY case} \\ 165 & \text{non-SUSY case.} \end{cases} \tag{26}$$

That is, the upper (lower) limit comes from the renormalizability of both top and bottom Yukawa coupling at GUT (low energy) scale [40]. For a non-SUSY model, the upper limit can be as large as 165. As will be shown in Sec. IV, we note that the RHC regions to be studied are $\langle\lambda\rangle \approx 10^{-7}$ and $\langle\eta\rangle \approx 10^{-10}$. If we adopt the approximation (22), one may get

$$\lambda \approx \left(\frac{M_1}{M_2}\right)^2 \text{ and } \eta \approx -\tan\zeta \approx \left(\frac{M_L^2}{M_R^2}\right)\frac{1}{\tan\beta} \approx \frac{\lambda}{\tan\beta}. \tag{27}$$

III. RHC DOUBLE BETA DECAY NUCLEAR MATRIX ELEMENTS FOR THE GROUND 0^+ AND EXCITED 2^+ STATES

A. Transition amplitude of 0ν DBD

The transition amplitude $I \to F + e_{p_1,s_1} + e_{p_2,s_2}$ is given by the second-order perturbation of H_W following Ref. [41]:

$$\begin{aligned} R_{0\nu} = {} & \frac{4}{\sqrt{2}}\left(\frac{G\cos\theta_c}{\sqrt{2}}\right)^2 \sum_{\alpha,\beta,i}\int d\boldsymbol{x}d\boldsymbol{y}\int \frac{d\boldsymbol{k}}{(2\pi)^3}e^{-i\boldsymbol{k}\cdot\boldsymbol{r}}\frac{-1}{2\omega} \\ & \times \left[\left(\bar{e}_{\boldsymbol{p}_2,s_2}(\boldsymbol{y})\gamma^\mu P_\beta(\gamma_0\omega - \boldsymbol{\gamma}\cdot\boldsymbol{k} + m_i)P_\alpha\gamma^\nu e^c_{\boldsymbol{p}_1,s_1}(\boldsymbol{x})\right)\left(\langle F|\tilde{J}_\beta^{\nu\dagger}(\boldsymbol{y})\frac{1}{E_I - (H_{st} + \omega + e_1)}\tilde{J}_\beta^{\mu\dagger}(\boldsymbol{x})|I\rangle\right)\right. \\ & \left. - \left(\bar{e}_{\boldsymbol{p}_2,s_2}(\boldsymbol{y})\gamma^\mu P_\beta(\gamma_0\omega + \boldsymbol{\gamma}\cdot\boldsymbol{k} - m_i)P_\alpha\gamma^\nu e^c_{\boldsymbol{p}_1,s_1}(\boldsymbol{x})\right)\left(\langle F|\tilde{J}_\beta^{\nu\dagger}(\boldsymbol{y})\frac{1}{E_I - (H_{st} + \omega + e_2)}\tilde{J}_\beta^{\mu\dagger}(\boldsymbol{x})|I\rangle\right)\right]. \end{aligned} \tag{28}$$

Here the four-momentum of the exchanged neutrino is $k^\mu = (\omega, \boldsymbol{k})$, $\boldsymbol{r} = \boldsymbol{x} - \boldsymbol{y}$, e_i is energy of the electron, and $\omega = (\boldsymbol{k}^2 + m_\nu^2)^{1/2}$. $|I\rangle$, $|F\rangle$ are state vectors of the initial and final hadron states and H_{st} is the Hamiltonian of the strong interaction. It is noticed that, at this stage the hadron current $\tilde{J}_\alpha^\mu$ is given in terms of current quark and initial and final state vector can be nuclear states or any hadronic states.

To simplify the derivation, we assume that the neutrino energy ω dominates the energy denominator $E_I - (H_{st} + \omega + e_i)$. $R_{0\nu}$ is then expressed as

$$R_{0\nu} = \frac{i}{4\pi}\frac{4}{\sqrt{2}}\left(\frac{G\cos\theta_c}{\sqrt{2}}\right)^2 \langle F|\mathcal{M}|I\rangle, \tag{29}$$

with

$$\mathcal{M} = \sum_{\alpha,\beta,i}\int d\boldsymbol{x}d\boldsymbol{y}\frac{h(r)}{r^2}\bar{e}_{\boldsymbol{p}_2,s_2}(\boldsymbol{y})/\tilde{J}^\dagger_\beta(\boldsymbol{y})P_\beta(\boldsymbol{r}\cdot\boldsymbol{\gamma})P_\alpha/\tilde{J}^\dagger_\alpha(\boldsymbol{x})e^c_{\boldsymbol{p}_1,s_1}(\boldsymbol{x}). \tag{30}$$

Here $h(r)$ is given as

$$h(r) = -\frac{4\pi}{(2\pi)^3}\, r\frac{d}{dr}\int d\boldsymbol{k}\frac{e^{-i\boldsymbol{k}\cdot\boldsymbol{r}}}{\omega^2} \sim \frac{1}{r}. \tag{31}$$

Now, the η and λ dependence of $\mathcal{M}$ are clearly given as

$$\mathcal{M} = \int d\boldsymbol{x}d\boldsymbol{y}\frac{h(r)}{r^2}\bar{e}_{\boldsymbol{p}_2,s_2}(\boldsymbol{y})\mathcal{O}e^c_{\boldsymbol{p}_1,s_1}(\boldsymbol{x}), \tag{32}$$

with

$$\begin{aligned}\mathcal{O} = {}& \langle\eta\rangle\{[\not{V}(\boldsymbol{y})(\boldsymbol{r}\cdot\boldsymbol{\gamma})\not{V}(\boldsymbol{x}) + \not{A}(\boldsymbol{y})(\boldsymbol{r}\cdot\boldsymbol{\gamma})\not{A}(\boldsymbol{x})] - [\not{V}(\boldsymbol{y})(\boldsymbol{r}\cdot\boldsymbol{\gamma})\not{A}(\boldsymbol{x}) + \not{A}(\boldsymbol{y})(\boldsymbol{r}\cdot\boldsymbol{\gamma})\not{V}(\boldsymbol{x})]\} \\ & + \langle\lambda\rangle\{[\not{V}(\boldsymbol{y})(\boldsymbol{r}\cdot\boldsymbol{\gamma})\not{V}(\boldsymbol{x}) - \not{A}(\boldsymbol{y})(\boldsymbol{r}\cdot\boldsymbol{\gamma})\not{A}(\boldsymbol{x})] - [\not{V}(\boldsymbol{y})(\boldsymbol{r}\cdot\boldsymbol{\gamma})\not{A}(\boldsymbol{x}) - \not{A}(\boldsymbol{y})(\boldsymbol{r}\cdot\boldsymbol{\gamma})\not{V}(\boldsymbol{x})]\gamma_5\}.\end{aligned} \tag{33}$$

The difference between the $\langle\eta\rangle$ and $\langle\lambda\rangle$ terms is seen in the different relative sings between the VV and the AA and also in those between the VA and the AV, with V and A being the vector and axial vector currents. Furthermore, γ_5 of the $\langle\lambda\rangle$ term modifies the even-odd structure of the lepton Dirac matrix. The formula can be used both for $0^+ \to 0^+$ and $0^+ \to 2^+$ nuclear DBD. Since the angular momentum $L = 1$ and parity -1 are carried by the neutrino, the $s_{1/2}$ and $p_{1/2}$ partial waves of the electron contribute to the $0^+ \to 0^+$ transition. However, as studied in Ref. [42] and discussed in Ref. [27], the magnetization current $\boldsymbol{\nabla}\times\boldsymbol{\mu}$ with the $(s_{1/2})^2$ electrons enhances the sensitivity of the η term through the $V-A$ interference term.

The enhancement mechanism of the $\langle\eta\rangle$ term for $0^+ \to 0^+$ DBD does not work for $0^+ \to 2^+$. In order to carry $J = 2$, electrons have to be at least $s_{1/2}$ and $p_{3/2}$ orbits. Sensitivity of the $\langle\eta\rangle$ term is similar to that of $\langle\lambda\rangle$ term for $0^+ \to 2^+$ DBD, while $0^+ \to 0^+$ DBD is particularly sensitive to the $\langle\eta\rangle$ term.

B. Effective operator for $0^+ \to 2^+$ transition

The outline of the derivation of the transition amplitude of angular momentum $J = 2$ of RHC DBD is briefly described. Using standard partial wave expansion of the scattering wave functions of electrons [43], the leading-order contribution of $s_{1/2}$ and $p_{3/2}$ states are taken as follows:

$$\bar{e}_{p_2,s_2}(\boldsymbol{y}) = \chi^\dagger_{s_2}[g^*_{-1}(p_2,y),\ -f^*_1(p_2,y)(\hat{p}_2\cdot\boldsymbol{\sigma})], \tag{34}$$

$$e^c_{p_1,s_1}(\boldsymbol{x}) = \begin{pmatrix} -if^*_2(p_1,x)[3(\hat{x}\cdot\hat{p}_1)(\hat{p}_1\cdot\boldsymbol{\sigma}) - (\hat{x}\cdot\boldsymbol{\sigma})] \\ ig^*_{-2}(p_1,x)[3(\hat{x}\cdot\hat{p}_1) - (\hat{x}\cdot\boldsymbol{\sigma})(\hat{p}_1\cdot\boldsymbol{\sigma})]\end{pmatrix}\chi^c_{s_1}, \tag{35}$$

with $\chi^c_s = i\sigma_2\chi_s$. $\hat{x}$ is a unit vector $\boldsymbol{x}/|\boldsymbol{x}|$. Matrix element $\mathcal{M}$ is given by the sum of each electron wave function as

$$\mathcal{M} = \mathcal{M}^{-2-1} + \mathcal{M}_{21} + \mathcal{M}_2{}^{-1} + \mathcal{M}^{-2}_1. \tag{36}$$

Here $\mathcal{M}^{ij}$ includes the electron wave function f^i_j defined in Ref. [41] where a superscript i (a subscript j), etc., indicate that $g^{(-)}_i$ ($f^{(-)}_j$) should be taken. For example, $f^{-2-1} = g_{-2}(p_1,R)g_{-1}(p_2,R)$, where R is the nuclear radius. f^{-2-1} and f_{21} contribute to the phase-space factor G_1, while $f_2{}^{-1}$ and f^{-2}_1 contribute to G_2. G_1 and G_2 are defined in Refs. [44,45]. $\mathcal{M}^{-2-1}$ and $\mathcal{M}_{21}$, which are the odd elements of the Dirac matrix $\mathcal{O}$, give effective rank 2 operators of $\langle\lambda\rangle M_\lambda - \langle\eta\rangle M_\eta$. $\mathcal{M}_2{}^{-1}$ and $\mathcal{M}^{-2}_1$ from the even element of $\mathcal{O}$ give $\langle\eta\rangle M'_\eta$.

Matrix elements $\mathcal{M}^{-2-1}$ and $\mathcal{M}_2{}^{-1}$ are given as

$$\mathcal{M}^{-2-1} = -i\frac{f^{-2-1*}}{R}\int d\boldsymbol{x}d\boldsymbol{y}\frac{h(r)}{r^2}\chi^\dagger_{s_2}[\langle\eta\rangle(M_{VV}+M_{AA}) + \langle\lambda\rangle(M_{VV}-M_{AA}+M_{VA-})][3(\boldsymbol{x}\cdot\hat{p}_1) - (\boldsymbol{x}\cdot\boldsymbol{\sigma})(\hat{p}_1\cdot\boldsymbol{\sigma})]\chi^c_{s_1}, \tag{37}$$

$$\mathcal{M}_2{}^{-1} = i\frac{f_2{}^{-1*}}{R}\int d\boldsymbol{x}d\boldsymbol{y}\frac{h(r)}{r^2}\chi^\dagger_{s_2}\langle\eta\rangle M_{VA+}[3(\boldsymbol{x}\cdot\hat{p}_1)(\hat{p}_1\cdot\boldsymbol{\sigma}) - (\boldsymbol{x}\cdot\boldsymbol{\sigma})]\chi^c_{s_1}, \tag{38}$$

where $M_{VV}, M_{AA}, M_{VA\pm}$ are

$$M_{VV} = V_0(\boldsymbol{y})\boldsymbol{r}\cdot\boldsymbol{\sigma}V_0(\boldsymbol{x}), \tag{39}$$

$$M_{AA} = [\boldsymbol{A}(\boldsymbol{y})\cdot\boldsymbol{\sigma}](\boldsymbol{r}\cdot\boldsymbol{\sigma})[\boldsymbol{A}(\boldsymbol{x})\cdot\boldsymbol{\sigma}], \tag{40}$$

$$M_{VA\pm} = V_0(\boldsymbol{y})(\boldsymbol{r}\cdot\boldsymbol{\sigma})[\boldsymbol{A}(\boldsymbol{x})\cdot\boldsymbol{\sigma}] \pm [\boldsymbol{A}(\boldsymbol{y})\cdot\boldsymbol{\sigma}](\boldsymbol{r}\cdot\boldsymbol{\sigma})V_0(\boldsymbol{x}). \tag{41}$$

Rewriting $\mathcal{M}$, the multipole operator for hadrons is written as the product of hadron and lepton irreducible tensors of rank 2. Here we show $\mathcal{M}^{-2-1}$, which include a necessary operator for the DBD of Δ_{1232}. The matrix element is rewritten in terms of hadron tensor $\mathcal{H}$ and lepton tensor $\mathcal{L}$ of rank $J = 2$ as

$$\mathcal{M}^{-2-1} = -i\frac{f^{-2-1^*}}{R}\frac{3\sqrt{5}}{2}[\mathcal{H}\otimes\mathcal{L}]^{(0)}, \quad \mathcal{M}_2{}^{-1} = i\frac{f_2{}^{-1^*}}{R}\frac{3\sqrt{5}}{2}[\mathcal{H}'\otimes\mathcal{L}']^{(0)}. \tag{42}$$

The lepton tensor, which is independent of nuclear coordinates, is

$$\mathcal{L} = \chi^\dagger_{s_2}[\hat{p}_1\otimes\boldsymbol{\sigma}]^{(2)}\chi^c_{s_1}, \quad \mathcal{L}' = \chi^\dagger_{s_2}\left([\hat{p}_1\otimes\hat{p}_1]^{(2)} + \sqrt{\frac{3}{2}}\left[[\hat{p}_1\otimes\hat{p}_1]^{(2)}\otimes\boldsymbol{\sigma}\right]^{(2)}\right)\chi^c_{s_1}, \tag{43}$$

and the hadron tensor is

$$\mathcal{H} = \langle\eta\rangle[h_{VV} + h_{AA}] - \langle\lambda\rangle[-h_{VV} + h_{AA} - h_{VA-}], \quad \mathcal{H}' = \langle\eta\rangle h_{VA+}. \tag{44}$$

Here

$$h_{VV} = \int d\boldsymbol{x}d\boldsymbol{y}h(r)V_0(\boldsymbol{y})V_0(\boldsymbol{x})[\hat{r}\otimes\hat{r}]^{(2)}, \tag{45}$$

$$h_{AA} = \int d\boldsymbol{x}d\boldsymbol{y}h(r)\left(\frac{2}{3}[\boldsymbol{A}(\boldsymbol{y})\otimes\boldsymbol{A}(\boldsymbol{x})]^{(2)} - \frac{1}{3}\boldsymbol{A}(\boldsymbol{y})\cdot\boldsymbol{A}(\boldsymbol{x})[\hat{r}\otimes\hat{r}]^{(2)} - \sqrt{\frac{7}{3}}[[\boldsymbol{A}(\boldsymbol{y})\otimes\boldsymbol{A}(\boldsymbol{x})]^{(2)}\otimes[\hat{r}\otimes\hat{r}]^{(2)}]^{(2)}\right), \tag{46}$$

$$h_{VA-} = -\sqrt{\frac{3}{2}}\int d\boldsymbol{x}d\boldsymbol{y}h(r)\left[[V_0(\boldsymbol{y})\boldsymbol{A}(\boldsymbol{x}) + \boldsymbol{A}(\boldsymbol{y})V_0(\boldsymbol{x})]\otimes[\hat{r}\otimes\hat{r}]^{(2)}\right]^{(2)}, \tag{47}$$

$$h_{VA+} = \int d\boldsymbol{x}d\boldsymbol{y}h(r)\frac{r_+}{r}\left[[V_0(\boldsymbol{y})\boldsymbol{A}(\boldsymbol{x}) - \boldsymbol{A}(\boldsymbol{y})V_0(\boldsymbol{x})]\otimes\left(\frac{1}{\sqrt{2}}[\hat{r}\otimes\hat{r}_+]^{(1)} - \sqrt{\frac{3}{2}}[\hat{r}\otimes\hat{r}_+]^{(2)}\right)\right]^{(2)}, \tag{48}$$

with $\boldsymbol{r}_+ = \boldsymbol{x} + \boldsymbol{y}$.

Taking the impulse approximation of the nuclear current $V_0(\boldsymbol{x}) = \sum_i \tau_i^+\delta(\boldsymbol{r}_i - \boldsymbol{x})$ and $\boldsymbol{A}(\boldsymbol{x}) = \sum_i g_{\rm A}\tau_i^+\boldsymbol{\sigma}_i\delta(\boldsymbol{r}_i - \boldsymbol{x})$, the half-life [44,45] is

$$(T_{1/2})^{-1} = G_1|\langle\lambda\rangle M'_\lambda - \langle\eta\rangle M'_\eta|^2 + G_2|\langle\eta\rangle M'_{\eta'}|^2, \tag{49}$$

where

$$M'_\lambda = \sum_{i=1}^{5} C_{\lambda i}M_i, \quad M'_\eta = \sum_{i=1}^{5} C_{\eta i}M_i, \quad M'_{\eta'} = \sum_{i=6}^{7} C'_{\eta i}M_i. \tag{50}$$

We refer the coefficients C_{xi} and C'_{xi} to Refs. [44,45]. The axial vector coupling constant $g_{\rm A}^4$ is included in the phase space factor G_i.

C. Estimation of $N\Delta$ transition in 0ν double beta decay

The hadron currents $J^\mu_{\rm L}$ and $J^\mu_{\rm R}$ are given in terms of current quarks. In the standard nuclear physics approach, the nuclear state vector is described using only nucleon degrees of freedom, instead of quarks. Therefore, an effective DBD interaction Hamiltonian has to be described by using nucleon degrees of freedom. This is achieved in two steps. At first, the semileptonic interaction is truncated into hadron degrees of freedom. The interaction Hamiltonian consists of nucleon current and $N\Delta$ transition current and possible weak pion production current as shown in the left panel of Fig. 1.

In the second step, hadron degrees of freedom other than nucleon are eliminated, and the effective Hamiltonian to be used with the many-body wave function of nucleons is obtained. The resultant effective semileptonic Hamiltonian is well known for beta decay, muon capture, and neutrino reactions. The nuclear weak current consists of one-nucleon impulse current (IMP) and many-body meson exchange current (MEC):

$$J^\mu(\boldsymbol{x}) = J^\mu_{\rm IMP}(\boldsymbol{x}) + J^\mu_{\rm MEC}(\boldsymbol{x}). \tag{51}$$

The contribution of Δ appears as MEC. The basic mechanism of DBD due to nuclear weak current in Eq. (51) is the neutrino exchange between nucleons shown in the right panel of Fig. 1, which includes IMP and MEC ($2N$ mechanism). The MEC of the axial vector current contributes partly to the quenching of

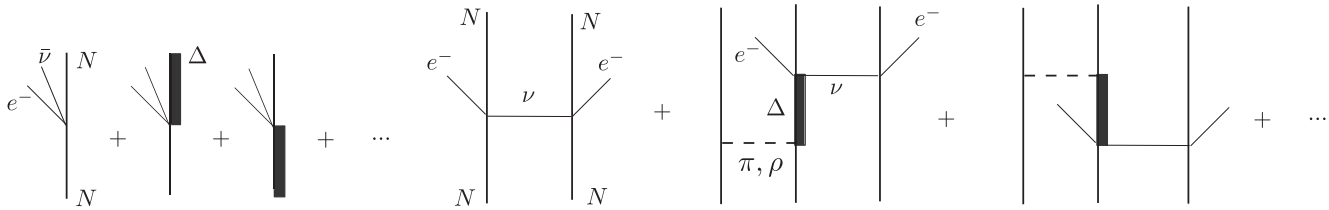

FIG. 1. Semileptonic interaction of hadron. Left panel shows electron and neutrino production processes of nucleon and $N \leftrightarrow \Delta$ transition. Right panel shows the $2N$ mechanism of DBD.

g_A seen in beta decay [12,46]. Since the high momentum will be carried by the exchanged neutrino in DBD compared with beta-decay and 2ν DBD, $g_A^{\rm eff}$ might depend on the kinematics of the process. Instead of $g_A^{\rm eff}$, the MEC in DBD has been studied in chiral effective field theory (EFT) [6,47]. The MEC of EFT includes more than Δ excitation shown in the right panel of Fig. 1. The MEC is estimated with the effective one-body current obtained by applying the "normal ordering" and is shown to give an important mechanism of the reduction of the Gamow-Teller transition. Here, we concentrate on the Δ mechanism which emerges in DBD as shown in the left panel of Fig. 2 [1,41]. Neutrino is exchanged between quarks within single hadron. This mechanism generates new MEC, as shown in the right panel of Fig. 2. Among the excited nucleon states, resonance must be an iso-spin 3/2 Δ resonance. $\Delta_{33}(1232)$ is expected to give the largest contribution. Then $N\Delta$ DBD contributes for $0^+ \to 2^+$ transition (Δ mechanism) but not for $0^+ \to 0^+$ transitions.

Within the nonrelativistic constituent quark model with SU(6) symmetry, the matrix element of h_{AA} for the $n \to \Delta^{++}$ transition is given as

$$\mathcal{M}_\Delta = \langle \Delta^{++}||h_{AA}||n\rangle = \langle \Delta^{++}|\left|\sum_{i,j=1}^{3}\frac{2}{3}[\boldsymbol{\sigma}_i \otimes \boldsymbol{\sigma}_j]^{(2)}h(r_{ij})\right||n\rangle$$
$$= -\frac{8\sqrt{10}}{3}\langle h\rangle, \tag{52}$$

where the first term of h_{AA} in Eq. (46) in terms of the quark operator contributes. The Δ mechanism contributes to both the η and λ terms.

The Δ mechanism is estimated in Ref. [1]. They give a large contribution of the Δ mechanism. It is estimated by using the probability of Δ in the nuclear wave function $P(\Delta)$ and the transition matrix element of the $A-1$ nucleons $\langle \Phi_F|\Phi_I\rangle$. $P(\Delta)$ is estimated as $P(\Delta) \approx 0.01$ following Ref. [48] based on the probability of iso-spin 1/2 N^* resonances instead of Δ, as suggested by the analysis of magnetic moment and the (p,d) reaction at that time. The transition matrix element is assumed to be $\langle \Phi_F|\Phi_I\rangle \approx \sqrt{0.1}$. Using those numbers, the Δ mechanism is estimated as

$$\frac{\langle 2^+||h_{AA}||0^+\rangle}{|\mathcal{M}_\Delta|} = \sqrt{P(\Delta)}\langle \Phi_F|\Phi_I\rangle \approx 3.2\times 10^{-2}. \tag{53}$$

The Δ mechanism is studied in the microscopic model for the DBD of ^{76}Ge in Ref. [44]. The Δ component in nuclei is evaluated perturbatively by using the transition potential $V_{NN\leftrightarrow N\Delta}$,

$$\langle 2^+||h_{AA}||0^+\rangle = \langle F||V_{NN-N\Delta}\frac{1}{E_f - H}\langle \Delta|h_{AA}|N\rangle$$
$$+ \langle N|h_{AA}|\Delta\rangle\frac{1}{E_i - H}V_{N\Delta-NN}||I\rangle. \tag{54}$$

The NN- $N\Delta$ transition potential is given by the pion and rho meson exchange model. The energy denominator is approximated by the $N\Delta$ mass difference $E_{i/f} - H \sim m_N - m_\Delta$. The Δ mechanism is evaluated by the meson-exchange current in Fig. 2 with a "Hartree-Fock-Bogoliubov–type" nuclear wave function. The Δ mechanism of the microscopic model turns out to be about 1/60 of the estimation of (53). The contribution of the Δ mechanism is not very large compared with the usual $2N$ mechanism [49].

The dominant contribution of the Δ mechanism is due to the matrix element of the following operator:

$$\sum_{m,n=1}^{A}\tau_m^+\tau_n^+\boldsymbol{\sigma}_m\cdot\boldsymbol{\sigma}_n[\hat{r}_{mn}\otimes\hat{r}_{mn}]^{(2)}. \tag{55}$$

The ratio of the NME of operators that have the same spin and angular momentum structure for both the $2N$ and Δ mechanism gives us a less-model-dependent estimation of the Δ mechanism. Using the notation of Ref. [44], M_1 is for the $2N$ mechanism, and M_9 and M_{12} are for the Δ mechanism. Apart from coupling constants, the difference among the matrix elements M_i is only the radial dependence of the operators, which is $h(r)$ for the $2N$ mechanism while that of the Δ mechanism with one-pion exchange is $Y_2(m_\pi r) = e^{-m_\pi r}[1 + 3/(m_\pi r) + 3/(m_\pi r)^2]/r$. Using the numbers of Ref. [44], the ratio is calculated as

$$r = \frac{C_{\lambda 1}M_1}{c_9 M_9 + c_{12}M_{12}} \approx 0.12. \tag{56}$$

Assuming the A dependence of the radial overlap integral is weak, the Δ mechanism for this particular type of matrix element is estimated as about 10% of that of the $2N$ mechanism

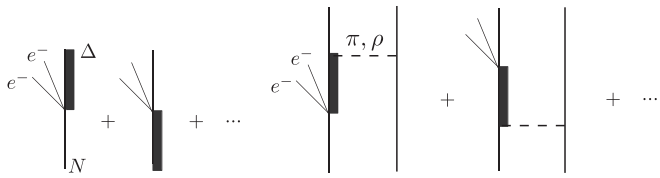

FIG. 2. Diagrams of neutrino exchange within a baryon. The left panel shows 0ν DBD of the $N \leftrightarrow \Delta$ transition. The right panel shows the Δ mechanism of DBD.

using $g_A = 1.27$, while the Δ mechanism can be 20% using quenched $g_A^{\rm eff} \approx 0.7$ [46].

IV. RIGHT-HANDED WEAK CURRENTS TO BE STUDIED BY TON-SCALE DOUBLE BETA DECAY EXPERIMENTS

We discuss first DBD rates for the individual RHC processes, i.e., the $\langle\lambda\rangle$ and $\langle\eta\rangle$ dominant cases, to see how the rates depend on $\langle\lambda\rangle$ and $\langle\eta\rangle$. The rate $\Gamma_k^{(J)}$ with k being λ and η for the $0^+ \to 0^+$ ground-state ($J = 0$) and the $0^+ \to 2^+$ excited state ($J = 2$) transitions are given as in Eqs. (11) and (49) and in Refs. [1,8,16,50] as

$$\Gamma_k^{(J)} = C_{kk}^{(J)}(\langle k\rangle)^2, \tag{57}$$

where $C_{kk}^{(J)}$ is the sensitivity to the k-mode DBD. The sensitivity is a kind of amplification factor to make the small $\langle k\rangle$ BSM visible experimentally. Actually, $C_{kk}^{(J)}$ is given by $\Sigma_i G_{kk}^{(J)}(i)[M_{kk}^{(J)}(i)]^2$ with $G_{kk}^{(J)}(i)$ and $[M_{kk}^{(J)}(i)]$ being the relevant $\beta\beta$ phase-space factors and the relevant NMEs. They correspond, respectively, to the atomic and nuclear amplification factors. The axial-vector weak coupling factor of g_A^4, where g_A is the axial-vector coupling in units of the vector coupling of g_V for a free nucleon, is conventionally included in $G_{kk}^{(J)}$.

The phase-space factor $G_{kk}^{(J)}(i)$ depends on the DBD Q value and the atomic number Z of the DBD nucleus and is rather well calculated in past and also in recent works [1,45,51,52]. The DBD NME is known to be rather sensitive to the nuclear models and the nuclear parameters used for the model calculation [16]. The NMEs involved in RHCs include various kinds of spin (σ) and isospin (τ) components, which depend strongly on the nuclear and non-nuclear $\sigma\tau$ correlations. Then the $\sigma\tau$ NMEs are known to be strongly quenched due to the $\sigma\tau$ correlations. Accordingly, the effective axial-vector coupling of $g_A^{\rm eff}$ is used for the model NME to incorporate such quenching effects as the nuclear medium effects and the non-nucleonic $\sigma\tau$ correlation effects that are not included explicitly in the model NME.

Recently $g_A^{\rm eff}/g_A$ is shown to be around 0.55 by analyzing the single-β decay rates and the summed $\sigma\tau$ strength in medium-heavy nuclei [46,53].

The DBD rates for the RHCs are evaluated for typical DBD nuclei of ^{76}Ge, ^{82}Se, ^{100}Mo, ^{130}Te, and ^{136}Xe. These nuclei are of current interest since good energy-resolution detectors and large amounts of the DBD isotopes are available, so future ton-scale experiments are under progress by using these isotopes [6,7].

The $\Gamma_k^{(0)}$ for the ground state is evaluated by using the NMEs based on the quasi-particle random phase approximation (QRPA) model [41,54] and the shell model [55], and $\Gamma_k^{(2)}$ for the excited 2^+ state by using the QRPA NMEs [45]. Note that these models take explicitly into account the $\sigma\tau$ and other correlations. Then the quenching coefficient of $g_A^{\rm eff}/g_A \approx 0.55$ [46,53] may be used to incorporate the nuclear medium and non-nucleonic $\sigma\tau$ correlations that are not included in their models.

The obtained RHC rates are shown in Fig. 3. $\Gamma_\lambda^{(0)}$ in units of 10^{-28} /yr for $\lambda = 1$ in units of 10^{-7} is around 10, while $\Gamma_\eta^{(0)}$ in the same units are of the order of 10^6, reflecting the much larger phase space factor of G_{09} for the recoil term involved in the η current for the ground-state decay, as discussed in Sec. III. On the other hand, $\Gamma_\lambda^{(2)}$ for $\lambda = 1$ in the same units is scattered around 1, and $\Gamma_\eta^{(2)}$ is scattered around 5. The ratio $\Gamma_\lambda^{(2)}/\Gamma_\lambda^{(0)} \approx 0.1$ reflects the ratio for their phase-space factors due to the smaller Q values for the excited states. We note that the RHC rates for the given λ and η are smaller for ^{76}Ge by an order of magnitude than those for others. The smaller rates are due to the smaller phase-space factors because of the smaller Q values for ^{76}Ge .

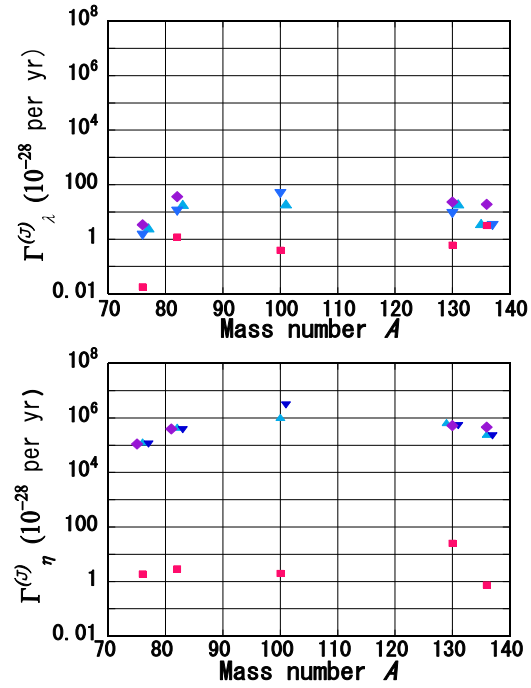

FIG. 3. RHC rates [($\Gamma_k = (C_{kk}$]) in units of 10^{-28} per year for RHC $k = 1$ in units of 10^{-7} for typical DBD nuclei of ^{76}Ge, ^{82}Se, ^{100}Mo, ^{130}Te, and ^{136}Xe of current interest. (top) $k = \langle\lambda\rangle$. (bottom) $k = \langle\eta\rangle$. NMEs used are the QRPA model NMEs in Ref. [54] (light-blue triangles), the QRPA model NMEs in Ref. [41] (blue inverse triangles), and the shell model NMEs in Ref. [55] (violet diamonds) for the ground-state (0^+) transitions and the QRPA NMEs in Ref. [45] for the excited 2^+ transitions (red squares). Some Γ_k points are shifted by the mass number 1 or 2 to avoid overlap with the others.

The ν mass of $\langle m\rangle$ and the RHCs of $\langle\lambda\rangle$ and $\langle\eta\rangle$ to be studied are beyond the standard model, and thus are considered to be very small if they are nonzero. No signals so far in 0ν DBD experiments with typical medium-heavy DBD nuclei suggest that the 0ν DBD rate for the ground-state transition is of the order of $\Gamma_k = 10^2$ /yr in units of 10^{-28} or less, i.e., $T_{1/2} \geqslant 10^{26}$ yr. This limit excludes the quasidegenerate effective ν mass of $\langle m\rangle \geqslant 100$ meV, depending on the NME. Thus next generation ton-scale DBD experiments are under-progress or planned to search for the DBDs in the region of the IH mass region of the effective ν mass around $\langle m\rangle \approx 0.3 \times 10^{-7}$ in units of m_e. This corresponds to the decay rate of $\Gamma_m = 1$ in units of 10^{-28} or less, i.e., $T_{1/2} \geqslant 10^{28}$ yr.

Now we discuss how the ton-scale detectors are used to access the new RHC region of interest. So, let us evaluate the minimum (i.e. the lower limit of) RHCs $\lambda_{\min}$ and $\eta_{\min}$ to be studied by the ton-scale experiments. They are obtained by requiring that the number of the DBD signals should exceed the fluctuation of the background signals, and thus depend on the detector specifications (number of isotopes, background rate, etc.) and the run time. The minimum RHC rates $\Gamma_{\min}$ in units of 10^{-28} to be studied by a DBD experiment are given as [16]

$$\Gamma_{\min}(d) = 2.4(A/100)d^2, \quad d = 1.3\epsilon^{-1/2}(B/NT)^{1/4}, \quad (58)$$

where A is the mass number of the DBD isotope, d is the sensitivity of the experiment with N-ton isotopes, B per t yr (ton year) backgrounds, and T yr (year) run time. The minimum RHC to be studied is given by $k_{\min} = (\Gamma_{\min}(d)/C_{kk})^{1/2}$. Note that $k_{\min}$ depends linearly on the NMEs in C_{kk} and the d, and thus very weakly on B/N to the power of $1/4$. It requires 100 times more N and 100 times less B to reduce the minimum RHC by a factor of 10.

The minimum RHC rate by a typical ton-scale DBD experiment for the DBD isotope with $A = 100$ and $d = 1$ with $N = 1$ t, $B = 1$ per t yr, $\epsilon = 0.7$, and $T = 5$ yr is $\Gamma_{\min}(1) = 2.4$ in units of 10^{-28} for both $\langle\lambda\rangle$ and $\langle\eta\rangle$ in the case of using typical calorimetric detectors to measure the sum of the two β rays.

We first consider DBD experiments with $d = 1$ and $\Gamma^{(J)} = 2.4$ for both the ground-state ($J = 0$) and excited-state ($J = 2$) transitions by such calorimetric detectors as to measure the total energy of the $\beta\beta$ rays and the γ ray. Note that the total energy for the excited-state transition is the same as that for the ground-state one. Then, the $\lambda_{\min}$ and $\eta_{\min}$ to be studied are shown in Fig. 5. Here we used the rates of $\Gamma_{\lambda}^{(J)} = 10$ and 1 for $J = 0$ and 2 in units of 10^{-28} for $\lambda = 1$ in units of 10^{-7}, and $\Gamma_{\eta}^{(J)} = 10^6$ and 5 for $J = 0$ and 2 in the same units (see Fig. 3).

The minimum RHCs to be studied with a typical ton-scale experiment with $d = 1$ is $\langle\lambda_{\min}\rangle \approx 0.5$ for the ground state and $\langle\lambda_{\min}\rangle \approx 1.5$ for the excited state, while $\langle\eta_{\min}\rangle \approx 1.5 \times 10^{-3}$ for the ground state and $\langle\eta_{\min}\rangle \approx 0.7$ for the excited state, all in units of 10^{-7}, as shown in the left and right panels of Fig. 4. These values reflect the square roots of the phase-space factors.$\langle\lambda_{\min}\rangle$ for the excited state is less stringent by a factor of 3 than that for the ground state but is used to confirm $\langle\lambda\rangle$ if observed in the ground-state transition, while $\langle\eta_{\min}\rangle$ for the excited state is too large to be observed since $\langle\eta\rangle$ itself is of the order of 10^{-9} or less. The DBD rate is proportional to the phase-space factor G, which is roughly proportional to Q^5, and the Q value for the excited state is about 2/3 of the ground state Q, and thus the DBD rate for the excited state is an order of magnitude smaller than that for the ground state if the NMEs are similar for both. Accordingly, the DBD to the excited state is, so far, considered to be of less discovery potential for exploring the RHC.

The present work shows that a better sensitivity (smaller d) measurement for the excited state is possible by measuring the γ ray from the 2^+ state in coincidence with the $\beta\beta$ rays to the 2^+ state. Noting that the β flight length is of the order of millimeters, while the γ one is of the order of centimeters, multicell (multisegmented) detectors are effective to separate

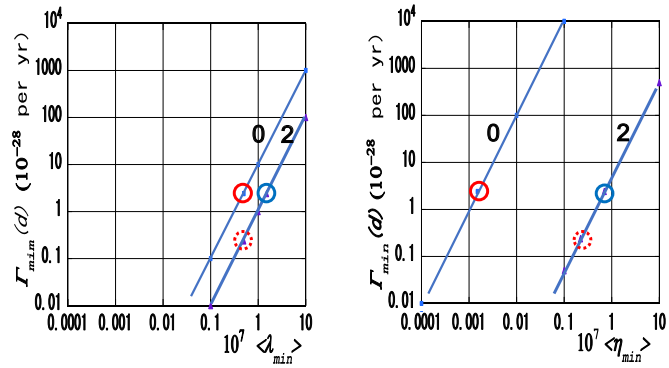

FIG. 4. The RHC rate Γ_k against the RHC $\langle k\rangle$ for the ground-state and the excited-state transitions. (left panel) $k = \lambda$. (right panel) $k = \eta$. (solid circles) Minimum RHCs to be studied by a typical ton-scale experiment of $d = 1$ without γ coincidence. (dotted circles) Those by a typical ton-scale experiment for $d = 0.3$ with $\beta\beta$-γ coincidence. See text.

the excited-state DBD followed by the γ ray from the ground-state DBD since the β-β starting at cell C_1 deposits their energies on the same cell C_1, while the γ ray may pass through cell C_1 and deposit the energy in cells C_i around cell C_1. Then the ground-state DBD is selected by setting the energy window at $E = Q$ for cell C_1 with the multiplicity = 1, while the excited-state DBD by the energy window at $E = Q'$ for the cell C_1 and the energy window at $E = E_\gamma$ for the summed signals from the nearby cells C_i. Thereby, the background is much reduced, depending on the energy window for the γ ray. The backgrounds from the 2ν DBD decay to the excited state is also much reduced by a factor of around $(Q'/Q)^{11} \approx 0.1$ than that for the ground-state transition. Backgrounds from solar neutrinos are also much reduced [56,57].

Actually, the background reduction rate depends strongly on the energy window, namely, the energy resolution of the γ measurement. It is evaluated to be of the order of $B'/B \approx 0.01$ in the case of bolometers with the energy resolution of around 10 keV. Then the detector sensitivity d gets smaller by a factor of around $(0.01)^{1/4} \approx 0.3$ by requiring coincidence with the γ ray, resulting in a smaller RHC rate and a smaller RHC by factors of around 0.1 and 0.3, respectively, as shown in the dotted circles. Then one can search for a similar $\langle\lambda\rangle$ region around 0.5 in units of 10^{-7} by both the ground-state and excited-state decays.

The region of the minimum RHCs of $\langle\lambda_{\min}\rangle$ and $\langle\eta_{\min}\rangle$ to be studied by the typical ton-scale experiment is shown in Fig. 5. Here we use the sensitivity of $d = 1$ for the ground-state transition and $d = 0.3$ for the excited-state transition by the β-γ coincidence. It is out of but close to the theoretically suggested region of $1 \leqslant \tan\beta \leqslant 165$ with $\tan\beta$ being around $\langle\lambda\rangle/\langle\eta\rangle$.

The regions of $\langle\lambda\rangle$ and $\langle\eta\rangle$ to be studied by the ton-scale DBD experiments of both the ground-state and excited-state decays are summarized as follows:

(A) The $\beta\beta$-γ coincidence measurement makes it possible to get the detector sensitivities around $d = 1$ for the ground-state decay with no γ coincidence and $d \approx 0.3$ for the excited-state decay with the γ coincidence.

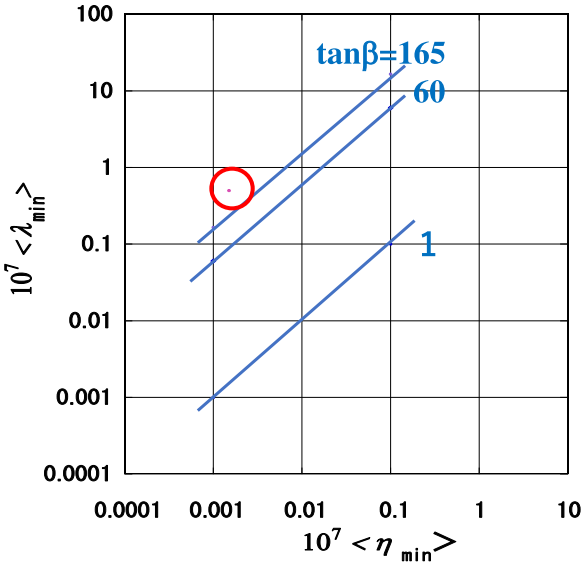

FIG. 5. (pink circle) The region around minimum RHCs of $\langle\lambda_{\rm min}\rangle$ and $\langle\eta_{\rm min}\rangle$ to be studied by a typical ton-scale experiment with a sensitivity of $d = 1$ and $d = 0.3$ for the ground- and excited-state decays. The solid lines show the lower bound of 1 and the upper bounds of 60 and 165 for tanβ, which is related to the order of the $\langle\lambda\rangle$-to-$\langle\eta\rangle$ ratio. See text.

(B) The $\langle\eta\rangle$ region above about 1.5×10^{-3} in units of 10^{-7} is well studied by searching for the $\beta\beta$ signals in the ground-state channel. No signals from $\langle\eta\rangle$ in the excited-state channel.

(C) The λ region above around 0.5 in units of 10^{-7} is exclusively studied by searching for the excited-state decay. If one observes nonzero signals in the excited-state window and no signal in the ground-state channel, the ratio of $\langle\lambda\rangle/\langle\eta\rangle$ is constrained to be of the order of 300 or larger, and the SUSY is disfavored. Thus, it provides experimentally the favored region of tanβ and the models behind it.

(D) In case of nonzero signals in both the ground- and excited-state windows, the signals in the ground state window may be due to both the λ and η currents. Here, the λ contribution in the ground-state window may in principle be evaluated from the rate in the excited-state channel if the RHC NMEs for both the ground- and excited-state decays are well established.

(E) In other words, the ratio $R(0/2)$ of the DBD rates for the ground 0^+ and excited 2^+ state decays is used to study exclusively the individual λ and η currents, $R(0/2) \gg 1$ leading to the η dominance and $R(0/2) \ll 1$ to the λ dominance. If we know the relevant NMEs well, the ratio is used to get the individual η and λ .

So far we have discussed the RHC rate using mainly the NMEs based on QRPA models with nuclear $\sigma\tau$ correlations and the quenched $g_{\rm A}^{\rm eff}$ with non-nuclear $\sigma\tau$ correlations. In fact, there are several models to evaluate the DBD NMEs, and the evaluated NMEs scatter over an order of magnitude, depending on the models [16]. Actually, the recent interacting boson model (IBM) NMEs [58] for the 2^+ RHCs are smaller by an order of magnitude than the QRPA ones. These smaller NMEs lead to $\langle\lambda_{\rm min}\rangle$ around 5 in units of 10^{-7} for the excited-state transition. Then one may have no DBD signal in the 2^+ window in the case of $\langle\lambda\rangle \approx 10^{-7}$.

It is noted that the transition amplitude (square root of the transition rate) of the NH ν mass term of $\langle m_\nu\rangle/m_e \approx 0.05$ is smaller by an order of magnitude than the amplitudes of the RHC $\langle\lambda\rangle \approx 0.5$ and $\langle\eta\rangle \approx 1.5 \times 10^{-3}$, all in units of 10^{-7}, to be studied by the ton-scale detector for the ground state transition. It is smaller by three orders of magnitude than that for the RHC $\langle\lambda\rangle \approx 0.5$ to be studied by the ton-scale detector for the excited-state transition [41,59]. Thus, almost no contributions from the ν mass term in the ton-scale experiment.

The possible regions of RHCs to be studied were discussed for simplicity for diagonal elements of $\Gamma_k^{(J)} = C_{kk}^{(J)}(\langle k\rangle)^2$ with k being λ and η, but the nondiagonal term of $C_{\lambda,\eta}(\langle\lambda\rangle\langle\eta\rangle)$ plays some role, depending on the NMEs, in case of the ground state transition with non zero λ and η currents.

V. CONCLUDING REMARKS

The present paper discusses new theoretical and experimental aspects of the RHCs of $\langle\lambda\rangle$ and $\langle\eta\rangle$ to be studied by the next-generation ton-scale DBD detectors. They are in progress to explore DBDs in the region of $T_{1/2} \approx 10^{-28}$ yr to search for the effective ν mass in the IH region. The ν mass spectrum, however, may likely be NH, and then no signal from the mass term. Then the detectors are used to explore the new regions of the RHCs.

On the basis of the left-right symmetric model, further theoretical discussions on the regions of the RHCs are made, and the order of the ratio $\langle\lambda\rangle/\langle\eta\rangle$ is shown to be given by tanβ, which is confined to be $1 \leqslant \tan\beta \leqslant 60, 165$, depending on the BSM models.

The NMEs involved in the RHCs have been explicitly given for both the 0^+ ground-state and 2^+ excited-state decays. The enhancement mechanism of the $\langle\eta\rangle$ term in the 0^+ transition has been clearly shown. The Δ mechanism with a ν exchange between quarks in Δ, which appears in the 2^+ decay, is shown to be about 20% of the $2N$ mechanism for the leading axial vector current NME of $\boldsymbol{\sigma}_m \cdot \boldsymbol{\sigma}_n Y_2$ in the case of a quenched $g_{\rm A}^{\rm eff} \approx 0.55 g_{\rm A}$ for the $2N$.

The new regions of RHCs are shown to be studied exclusively by measuring both the ground-state $\beta\beta$ decay followed by no γ ray, and the excited-state $\beta\beta$ decay followed by a γ ray. Here, multicell (segmented) detectors like bolometers are used to measure separately the $\beta\beta$ and the γ. Then the $\langle\lambda\rangle$ region above 0.5 in units of 10^{-7} and the $\langle\eta\rangle$ region above 1.5×10^{-3} in units of 10^{-7} are studied, and nonzero values for or limits on $\langle\lambda\rangle$, $\langle\eta\rangle$, and $\langle\lambda\rangle/\langle\eta\rangle$ give great impact on the BSM physics.

The RHCs to be studied are evaluated by using mainly QRPA NMEs with nucleonic $\sigma\tau$ correlations and the quenched coupling of $g_{\rm A}^{\rm eff}$ to incorporate the non-nucleonic $\sigma\tau$ correlations and others. Actually, the NMEs depend on the models and parameters used for the model as in the case of the NMEs for the ν mass mode. Needless to say, accurate theoretical and experimental evaluations for the λ and η NMEs are indispensable for quantitative studies of them.

It is encouraged to study RHCs on several nuclei to confirm the RHCs, if they are observed, in view of the uncertainties of the NMEs and the fluctuations of the backgrounds in the region of interest. They would help to identify the RHCs involved if the individual RHC NMEs were very accurately evaluated and their values were very different among the nuclei [27].

Alternatively, experimental studies of the 2^+ DBDs in more than two nuclei provide a unique opportunity to check if the NMEs are right or wrong since $\langle\lambda\rangle$, being the same among the nuclei, is only one BSM term involved in the L-R symmetry model.

The DBD detectors discussed in the present work are calorimetric detectors with high discovery potential. High-sensitivity ton-scale tracking detectors are of great interest to measure the β-β energy correlation to identify the individual λ and η currents [1,2,5,13,41,59].

ACKNOWLEDGMENTS

We are grateful to K. S. Babu and N. Okada for the comments on Eq. (26). This work was partly supported by JSPS KAKENHI Grant No. JP23K22508 (T.F.).

DATA AVAILABILITY

The data that support the findings of this article are not publicly available. The data are available from the authors upon reasonable request.

[1] M. Doi, T. Kotani, and E. Takasugi, Double beta decays and Majorana neutrino, Prog. Theor. Phys. Suppl. **83**, 1 (1985).
[2] H. Ejiri, Double beta decays and ν masses, J. Phys. Soc. Jpn. **74**, 2101 (2005).
[3] F. Avignone, S. Elliott, and J. Engel, Double beta decay, Majorana ν, and ν mass, Rev. Mod. Phys. **80**, 481 (2008).
[4] H. Ejiri, Double β-decays and ν nuclear responses, Prog. Part. Nucl. Phys. **64**, 249 (2010).
[5] J. Vergados, H. Ejiri, and F. Šimkovic, Theory of neutrinoless double-β-decay, Rep. Prog. Phys. **75**, 106301 (2012).
[6] M. Agostini, G. Benato, J. A. Detwiler, J. Menéndez, and F. Vissani, Toward the discovery of matter creation with neutrinoless $\beta\beta$ decay, Rev. Mod. Phys. **95** 025002 (2023).
[7] S. Umehara and H. Ejiri, Neutrino masses and right-handed weak currents studied by neutrino-less $\beta\beta$-decay detectors, Universe **10**, 247 (2024).
[8] J. Suhonen and O. Civitarese, Weak interaction and nuclear structure aspect of nuclear double beta decay, Phys. Rep. **300**, 123 (1998).
[9] A. Faessler and F. Simkovic, Double beta decay, J. Phys. G: Nucl. Part. Phys. **24**, 2139 (1998).
[10] J. Suhonen and O. Civitarese, Double-beta decay nuclear matrix elements in the pnQRPA framework, J. Phys. G: Nucl. Part Phys. **39**, 085105 (2012).
[11] J. Engel and J. Menéndez, Status and future of nuclear matrix elements for ν less double β-decay: A review, Rep. Prog. Phys. **80**, 046301 (2017).
[12] H. Ejiri, Nuclear matrix elements for β and $\beta\beta$ decays and quenching of the weak coupling g_A in QRPA, Front. Phys. **7**, 30 (2019).
[13] D. Štefánik, R. Dvornicky, F. Simkovic, and P. Vogel, Reexamining the light neutrino exchange mechanism of the $0\nu\beta\beta$ decay with left- and right-handed leptonic and hadronic currents, Phys. Rev. C **92**, 055502 (2015).
[14] H. Ejiri, Nuclear spin isospin responses for low-energy νs, Phys. Rep. **338**, 265 (2000).
[15] J. Suhonen, Impact of the quenching of g_A on the sensitivity of $0\nu\beta\beta$ experiments, Phys. Rev. C **96**, 055501 (2017).
[16] H. Ejiri, J. Suhonen, and K. Zuber, ν nuclear responses for astro-νs, single β-decays, and double β-decays, Phys. Rep. **797**, 1 (2019).
[17] T. Fukuyama, K. Ichikawa, and Y. Mimura, Revisiting fermion mass and mixing fits in the minimal SUSY $SO(10)$ GUT model, Phys. Rev. D **94**, 075018 (2016).
[18] A. G. Adame *et al.* (DESI Collaboration), Cosmological constraints from the measurements of baryon acoustic oscillations, J. Cosmol. Astropart. Phys. **2**, 021 (2025).
[19] N. Aghanim *et al.* (Planck Collaboration), Planck 2018 results. V. CMB power spectra and likelihoods, Astron. Astrophys. **641**, A5 (2020).
[20] F. J. Qu *et al.* (ACT Collaboration), The Atacama cosmology telescope: A measurement of the DR6 CMB lensing power spectrum and its implications for structure growth, Astrophys. J. **962**, 112 (2024).
[21] M. Sen and A. Y. Smirnov, Neutrinos with refractive masses and the DESI BAO results, arXiv:2407.02462.
[22] G. Li, M. J. Ramsey-Musolf, and J. C. Vasquez, Left right symmetry and leading contributions to neutrinoless double beta decays, Phys. Rev. Lett. **126**, 151801 (2021).
[23] H. Ejiri, N. Kamikubota, Y. Nagai, T. Nakamura, K. Okada, T. Shibata *et al.*, Double beta decay of ^{76}Ge$(0^+) \to 0^+$ and 2^+ states in ^{76}Se studied by the β-γ coincidence method, J. Phys. G **13**, 839 (1987).
[24] H. Ejiri, K. Fushimi, K. Hayashi, R. Hazama, T. Kishimoto, N. Kudomi *et al.*, Limits on neutrinoless double beta decay of ^{100}Mo, Nucl. Phys. A **611**, 85 (1996).
[25] T. Fukuyama, Y. Mimura, and Y. Uesaka, Neutrinoless double beta deacay and the muonium-to-antimuonium transition in models with doubly charged scalar, Phys. Rev. D **106**, 055041 (2022).
[26] T. Fukuyama, A. Ilakovac, T. Kikuchi, S. Meljanac, and N. Okada, SO(10) group theory for the unified model building, J. Math. Phys. **46**, 033505 (2005).
[27] T. Fukuyama and T. Sato, Neutrinoless double beta decay and $\langle\eta\rangle$ mechanism in the left-right symmetric model, J. High Energy Phys. 06 (2023) 049.
[28] P. Minkowski, $\mu \to e\gamma$ at a rate of one out of 10^9 muon decays? Phys. Lett. B **67**, 421 (1977).
[29] T. Yanagida, Horizontal gauge symmetry and masses of neutrinos, in *Proceedings of the Workshop on the Unified Theory and the Baryon Number in the Universe*, edited by O. Sawada and A. Sugamoto (Tsukuba, 1979), p. 95.

[30] M. Gell-Mann, P. Ramond, and R. Slansky, Complex spinors and unified theories, in *Supergravity*, edited by P. van Nieuwenhuizen and D. Freedman (NorthHolland, Amsterdam, 1979), p. 315.

[31] R. N. Mohapatra and G. Senjanovic, Neutrino mass and spontaneous parity nonconservation, Phys. Rev. Lett. **44**, 912 (1980).

[32] J. Kersten and A. Y. Smirnov, Right-handed neutrinos at CERN LHC and the mechanism of neutrino mass generation, Phys. Rev. D **76**, 073005 (2007).

[33] C. H. Lee, P. S. Bhupal Dev, and R. N. Mohapatra, Natural TeV-scale left-right seesaw mechanism for neutrinos and experimental tests, Phys. Rev. D **88**, 093010 (2013).

[34] F. Šimkovic, J. Vergados, and A. Faessler, Few active mechanisms of the neutrinoless double beta-decay and effective mass of Majorana neutrinos, Phys. Rev. D **82**, 113015 (2010).

[35] G. Pantis, A. Faessler, W. A. Kaminski, and J. D. Vergados, Description of the 0 neutrino beta decay of ^{48}Ca, ^{76}Ge, ^{100}Mo, ^{128}Te, ^{130}Te, J. Phys. G: Nucl. Part. Phys. **18**, 605 (1992).

[36] G. Pantis, F. Simkovic, J. D. Vergados, and A. Faessler, Neutrinoless double beta decay within QRPA with proton-neutron pairing, Phys. Rev. C **53**, 695 (1996).

[37] Y. Zhang, H. An, X. Ji, and R. N. Mohapatra, General CP violation in minimal left-right symmetric model and constraints on the right-handed scale, Nucl. Phys. B **802**, 247 (2008).

[38] For a review, P. Langacker, *The Standard Model and Beyond* (CRC Press, London, 2009).

[39] A. M. Sirunyan *et al.* (CMS Collaboration), Search for W′ bosons decaying to a top and a bottom quark at $\sqrt{s} = 13$ TeV in the hadronic final state, Phys. Lett. B **820**, 136535 (2021).

[40] B. Ananthanarayan, G. Lazarides, and Q. Shafi, Top-quark-mass prediction from supersymmetric grand unified theories, Phys. Rev. D **44**, 1613 (1991).

[41] T. Tomoda, Double beta decay, Rep. Prog. Phys. **54**, 53 (1991).

[42] T. Tomoda, A. Faessler, K. W. Schmid, and F. Grümmer, Neutrinoless double beta decay and a new limit on the lepton number violation, Phys. Lett. B **157**, 4 (1985).

[43] W. Horiuchi, T. Sato, Y. Uesaka, and K. Yoshida, Electron wave functions in beta-decay formulas revisited (I): Gamow-teller and spin-dipole contributions to allowed and first-forbidden transitions, PTEP **2021**, 103D03 (2021).

[44] T. Tomoda, $0^+ \to 2^+$ neutrinoless beta beta decay of ^{76}Ge, Nucl. Phys. A **484**, 635 (1988).

[45] D. L. Fang and A. Faessler, $0\nu\beta\beta$ decay to the first 2^+ state with a two-nucleon mechanism for a *L*-*R* symmetric model, Phys. Rev. C **107**, 015501 (2023).

[46] H. Ejiri, L. Jokiniemi, and J. Suhonen, Nuclear matrix elements for $\beta\beta$ decays and spin isospin giant resonances, Phys. Rev. C **105**, L022501 (2022).

[47] J. Menéndez, D. Gazit, and A. Schwenk, Chiral two-body currents in nuclei: Gamow-teller transitions and neutrinoless double-beta decay, Phys. Rev. Lett. **107**, 062501 (2011).

[48] H. Primakoff and S. P. Rosen, Nuclear double-beta decay and a new limit on lepton nonconservation, Phys. Rev. **184**, 1925 (1969).

[49] J. D. Vergados, A. Faessler, and T. Tomoda, The $\Delta(3/2, 3/2)$ contribution to the $0^+ \to 2^+\beta\beta$ decay transitions, Nucl. Phys. A **490**, 556 (1988).

[50] H. Ejiri, ν-mass sensitivity and nuclear matrix element for ν less double beta decay, Universe **6**, 225 (2020).

[51] J. Kotila and F. Iachello, Phase space factors for double beta decay, Phys. Rev. C **85**, 034316 (2012).

[52] S. Stoica and M. Mirea, Phase space factors for double beta decays, Front. Phys. **7**, 12 (2019).

[53] H. Ejiri, Delta-isobar resonance effects on nuclear matrix elements for neutrinoless $\beta\beta$ decays and astro- ν inverse- β decays, arXiv:2502.06122v1.

[54] K. Muto, E. Bender, and H. V. Klapdor, Effects of ground state correlations on $2\nu\beta\beta$ decay rates and limitations of the QRPA approach, Z. Phys. **334**, 187 (1989).

[55] D. L. Fang, B. A. Brown, and F. Simkovic, Nuclear shell model study of neutrinoless double beta decay under left-right symmetry model, arXiv:2407.02795v1.

[56] H. Ejiri and S. R. Elliott, Charged current neutrino cross sections for solar neutrinos, and background to $\beta\beta(0\nu)$ experiments, Phys. Rev. C **89**, 055501 (2014).

[57] H. Ejiri and S. R. Elliott, Solar neutrino interactions with the double-β decay nuclei of ^{82}Se, ^{100}Mo, and ^{150}Nd, Phys. Rev. C **95**, 055501 (2017).

[58] J. Ferretti, R. M. Vsevolodovna, J. Kotila, and E. Santopinsto, $O^+ \to 2^+$ neutrinoless double-β decay of ^{76}Ge, ^{82}Se, ^{130}Te, and ^{136}Xe in the microscopic interacting boson model, arXiv:2301.02007v1.

[59] T. Tomoda, $0^+ \to 2^+ 0\nu\beta\beta$ decays triggered directly by the Majorana neutrino mass, Phys. Lett. B **474**, 245 (2000).